Human Stress Response Specificity through Bioresonance Selectivity

Michael Worcester[1]†, Shayan Nejad[1]†, Devin O'Donnell[2], Surya Arian[3], Pratyasha Mishra[2], Arya Eimagh Naeini[1], Siyu Li[4], Kevin Yang[1], Aisa Anbir[2], Matthew Guevara[5], Nina Y. Yuan[6], Seán O'Leary[5], Marcus Kaul[6], Roya Zandi[1,2], and Thomas E. Kuhlman[1,2,3,5*]

Affiliations:

[1] Department of Physics and Astronomy, University of California, Riverside; Riverside, CA, 92521, USA.
[2] Biophysics Program, University of California, Riverside; Riverside, CA, 92521, USA.
[3] Microbiology Program, University of California, Riverside; Riverside, CA, 92521, USA.
[4] Department of Physics and Astronomy, California State Polytechnic University, Pomona; Pomona, CA, 91768, USA
[5] Department of Biochemistry, University of California, Riverside; Riverside, CA, 92521, USA.
[6] Division of Biomedical Sciences, School of Medicine, University of California, Riverside; Riverside, CA, 92521, USA.
† These authors contributed equally to this work.

*Corresponding author. Email: thomas.kuhlman@ucr.edu

Abstract:

In all eukaryotes, the mitogen activated protein kinase (MAPK) cascade, a multilayered interconnected network of enzymes, connects external stimuli to gene regulation, dictating cellular fate. However, mechanisms for encoding information in this complex, fluctuating network to activate specific responses remain elusive. Here, we demonstrate that the central human stress regulator protein p38 MAPK encodes information regarding experienced stresses as different frequency oscillations of its activation state. These oscillations are used to drive specific responses through frequency-dependent resonance of oscillating biochemical phosphorylation reactions between p38 and downstream targets. These interactions closely mirror those of electronic alternating current (AC) circuits and their components, providing a unique framework through which to understand signal transduction in the MAPK cascade. Finally, we demonstrate how this understanding of bioresonance allows us to induce specific genetic responses simply by exposing cells to sugar to force activation state oscillations of p38 at predetermined frequencies.

Introduction

Enzyme specificity is essential for the adaptability and survival of all living organisms. An example relevant to all eukaryotes is the mitogen activated protein kinase (MAPK) cascade, a complex network of dozens of enzymes responsible for sensing environmental stimuli and propagating the signal to the genome to alter gene expression. The cascade transmits received signals as a current of activating and deactivating phosphorylation reactions between MAPK enzymes. In the case of environmental stresses, the current starts from the stress receptors, is passed through the MAP3K and MAP2K layers of the cascade, and is ultimately received by the master stress response regulator protein p38 MAPK (*1, 2*). Once activated by dual phosphorylation at Thr-180 and Tyr-182 by the MAP2K enzymes MKK3 or MKK6 (*3*), p38 must then selectively phosphorylate and activate the correct substrates from a pool of hundreds of different possible protein targets. This initiates specific gene expression responses appropriate to the received stress (*2*). Selection of incorrect responses can be catastrophic, as inappropriate p38 activity is implicated in many devastating human diseases, including Alzheimer's disease (*4*), amyotrophic lateral sclerosis [ALS, (*5, 6*)], neuroHIV (*7, 8*), and cancer (*9, 10*), among many others (*1, 11*).

How can p38, which can exist in an active phosphorylated state or an inactive dephosphorylated state, encode enough information to provide specificity in response selection? In some cases, specificity in p38-target interactions is aided by allosteric control (*12*) and/or regulation of p38 and substrate availability or localization (*13-15*). However, because p38 regulates hundreds of targets, it is difficult to imagine how to generalize such approaches to form a comprehensive model of p38 selectivity due to the numbers of additional allosteric and localization effectors that would be required.

Extracting order from this complex network of interacting components is further complicated by dynamic temporal patterns and oscillations in number and activation state that have been observed in thousands of proteins within and associated with the MAPK cascade (*16*). These include the master regulator ERK1/2 (*17, 18*), the MAP2Ks MKK3 and MKK6 (*19-22*), and the transcription factors NF-κB (*23, 24*) and p53 (*25, 26*), among many others (*27*). Because the output of a particular signaling pathway relies on the balance between activation and deactivation by kinase and phosphatase enzymes, the temporal behavior of pathway components has been proposed to contribute to signaling specificity (*23, 24, 28*). However, specific mechanisms for how such temporal dynamics are interpreted or employed by signaling pathways remain largely obscure.

Results

VPC directly reports p38 activation state by FRET

Existing tools for studying the flow of information through the MAPK cascade and p38 rely upon indirect measurement of p38 activity. These include kinase translocation reporters (KTRs), which are kinase substrates that report kinase activity through fluorophore translocation into and out of the nucleus upon phosphorylation (*29*), and Förster resonance energy transfer based kinase substrates that change their FRET state when acted upon by the kinase of interest. Tomida *et al*. previously developed the FRET-based p38 substrate PerKy-38 (*30*), which is based upon the p38 docking domain of the transcription factor protein MEF2A and therefore acts as a MEF2A-like substrate for p38. However, p38 serves only to phosphorylate PerKy-38 and KTRs, while they are dephosphorylated independently by other phosphatases (*31, 32*). Hence PerKy-38 and KTRs report more accurately on the activation state dynamics and interactions of p38 substrates than those of p38 itself.

To overcome this limitation, we developed VPC (Venus-p38-Cerulean), which directly reports on p38 activation state by FRET, and we validated that the phosphorylation and activity dynamics of VPC are representative of native p38 on the time scales measured here. VPC is a translational fusion of the N and C terminal ends of p38α, the most ubiquitously expressed isoform of p38 (*33*), to the monomeric fluorescent reporters mVenus (*34*) and mCerulean3 (*35*). When human HEK-293T cells are stably transfected to express low levels of VPC, VPC displays patterns of intracellular localization upon stimulation that are consistent with observations of nuclear and cytoplasmic activity displayed by native p38 upon phosphorylation [**FIGURES 1A,B**; (*36*)]. VPC phosphorylation state dynamics measured by both western blot and ensemble-averaged FRET recapitulate those of p38 in untransfected HEK-293T cells (**FIGURE 1C**). Furthermore, the FRET signal of VPC purified from unstimulated cells increases when phosphorylated *in vitro* by the p38 kinase MKK6 (**FIGURE 1D, FIGURE S1B,C**). Finally, the FRET state of stimulated VPC-expressing cells changes dynamically in time (**FIGURE 1E**) and proportionally in amplitude (**FIGURE 1F**) in response to osmotic shocks of various strengths.

p38 and the TF-based p38 substrate PerKy-38 exhibit activation state oscillations

By measuring the FRET responses of both p38 and the transcription factor (TF)-based p38 substrate PerKy-38 in response to stimuli, we directly observe at the single cell level and in real time how information is passed between layers of the MAPK cascade. As the FRET level of each individual protein changes discretely when activated (**FIGURE 2A**), FRET levels measured from individual cells are proportional to the amount of activated PerKy-38 or VPC within those cells (**FIGURE 2B**). When stimulated, the activation states of both p38 and PerKy-38 oscillate in time (**FIGURE 2C**), corresponding to temporal waves in numbers of activated molecules.

The activation state of the TF-based p38 substrate PerKy-38 oscillates at a specific frequency when HEK-293T cells stably transfected to express PerKy-38 (henceforth PerKy293) are stimulated with the pro-inflammatory cytokine interleukin-1β (IL-1β), as reported previously (*30*). Example PerKy293 FRET time traces are shown in **FIGURE 2D**. The oscillatory response is eliminated upon treatment of the cells with SB203580 (**FIGURE S2**), a p38-specific inhibitor that binds to the p38 ATP binding pocket and prevents phosphorylation of downstream targets (*37*). To quantify the oscillations, we performed Fourier analysis on the FRET time traces of ~700 cells recorded over 48 hours [see **Supplementary Materials (SM) I**]. The ensemble averaged Fourier spectrum of the SB203580-treated PerKy293 control exhibits a smooth noise background (**FIGURE S2B,C**), and quantification of the statistics of the fluctuations away from power law behavior allows us to assign *p*-values and statistical significance to peaks observed in non-control spectra (see **SM II**, **FIGURE S2D**). For PerKy293 cells stimulated with IL-1β, we find the only statistically significant peak occurring at a frequency of $f = 0.36 \pm 0.02$ hr^{-1} ($p = 2.5 \times 10^{-13}$), corresponding to a period of ~2.8 hours (**FIGURE 2E**), consistent with Tomida *et al.*'s qualitatively determined period of 2 - 3 hours in HeLa cells (*30*). Conversely, we observe no PerKy-38 activity or oscillations when cells are exposed to SARS-CoV-2 Spike S1 subunit protein (**FIGURE 2F**) or when osmotically shocked by the addition of 120 mM sorbitol to the medium.

Direct measurement of the p38 activation state in HEK-293T cells stably transfected to express VPC (henceforth VPC293) also shows an oscillatory FRET response when stimulated with IL-1β (**FIGURE 2G**). However, unlike PerKy-38, p38 oscillations occur regardless of the specific stimulus used. As a control, cells transfected to express a combination of singly labeled Venus-p38 and p38-mCerulean3 ("VPPC293") show no FRET response (**FIGURE S3A**), and we again

analyzed the noise spectrum of this control (**FIGURE S3B-D, SM II**) to allow us to assign *p*-values and statistical significance to peaks observed in spectra obtained from VPC293 cells. Similarly to PerKy-38, he ensemble averaged Fourier spectrum decomposed from VPC293 cells stimulated with IL-1β displays a statistically significant peak at a frequency of 0.36 ± 0.02 hr^{-1} ($p = 4.6 \times 10^{-3}$), but additionally shows other significant peaks at 0.18 ± 0.02 hr^{-1} ($p = 2.9 \times 10^{-3}$) and 0.54 ± 0.02 hr^{-1} ($p = 3.1 \times 10^{-3}$) (**FIGURE 2H**). In contrast, when VPC293 cells are exposed to SARS-CoV-2 Spike S1, the VPC Fourier spectrum displays a statistically significant peak at a frequency of 0.45 ± 0.01 hr^{-1} ($p = 5.7 \times 10^{-4}$; **FIGURE 2I**). Hyperosmotic shock via the addition of 120 mM sorbitol to the medium results in a peak at a frequency of 0.54 ± 0.02 hr^{-1} ($p = 2.4 \times 10^{-4}$).

p38 activation state oscillates with stimulus-specific frequencies

As the above experiments suggest, when treating VPC293 cells with a variety of stimuli we observe p38 oscillatory spectra composed of different frequencies. Line spectra of detected frequencies for VPC293 cells stressed with various stimuli are shown in **FIGURE 2J,K**. Combining these individual spectra into a single aggregate spectrum (**FIGURE 2K**, top) shows that every detected frequency from all stimuli tested here are evenly spaced integer multiple harmonics of a fundamental frequency, f_0, such that the frequency of the nth harmonic is given by $f_n = (n+1)f_0$, with n an integer, $n = 0, 1, 2, ...$ Quantitative analysis of these frequencies extracts a best-fit fundamental frequency of $f_0 = 0.090 \pm 0.002$ hr^{-1} (see **SM III** and **FIGURES S4A,B**), and that up to the 12th harmonic is seen in our experiments. Comparison of the distribution of these frequencies with that expected from a collection of randomly distributed frequencies demonstrates that the data are distributed closer to evenly spaced harmonics than would be expected at random ($p = 0.004$; see **FIGURE 2L**, **FIGURE S4C**, **SM III**).

This demonstrates that various stimuli result in differential enhancement of stimulus-specific p38 harmonic frequencies, with the pro-inflammatory cytokine IL-1β (300 ng/mL) eliciting a complex spectrum including a mix of 1st, 3rd, and 5th harmonics, with weaker response of the 6th, 7th, and 11th, see **FIGURE 2K**, second row. Addition of SB203580 (10 μM) along with IL-1β (300 ng/mL) results in replacement of the 5th with the 4th, along with weak activation of the 8th (**FIGURE 2K**, third row). Conversely, stimulation with the multifunctional cytokine Tumor Necrosis Factor (TNF, 200 ng/mL) also results in a complex response, but with strong activation of the 3rd, 6th, and 12th, with weak activation of the 0th, 1st, 5th, and 9th, as shown in **FIGURE 2K**, fourth row. Stimulation with SARS-CoV-2 Spike S1 primarily activates the 0th and 4th harmonics (**FIGURE 2K**, fifth row), and hyperosmotic shock induced by addition of 120 mM sorbitol activates the 5th harmonic with weak activation of the 0th (**FIGURE 2K**, sixth row). Accordingly, for the stimuli tested here, we only observe a response in PerKy293 cells when stimulated with the cytokines IL-1β and TNF, which activate the 3rd harmonic at $f_3 = 0.36$ hr^{-1}, but do not observe a PerKy-38 response when stimulated with SARS-CoV-2 Spike S1 or hyperosmotic shock, *e.g.*, **FIGURE 2F**. The time dependence of the appearance of different frequencies can be complex (see **FIGURE S5**, **SM IV**), although here we focus on the time-averaged response.

p38 activates substrates through bioresonance

The Fourier spectra of p38 and PerKy-38 exhibit precisely the relationship expected between two oscillators coupled by resonance (*38*), where an oscillating target undergoes large amplitude

oscillations only when pumped by a driving force oscillating at the same natural frequency of the target (see **SM V, SM VI**). Here, p38 serves as the driving oscillator, while PerKy-38 acts as the target, with its natural oscillatory frequency of $f = 0.36$ hr^{-1} determined by interactions of PerKy-38 with p38, its phosphatases, and other proteins in this HEK-293T cell line (see **SM VI**). We call this phenomenon bioresonance to distinguish it from other unrelated uses of the term resonance in chemistry and biochemistry.

The relationship between the p38 and PerKy-38 spectra can be quantified by the transfer function, $\psi(\omega)$, which describes how the output oscillatory spectrum of the PerKy-38 target, $\tilde{x}(\omega)$, arises from coupling to the input oscillations of the p38 driver, $\tilde{y}(\omega)$, such that $\tilde{x}(\omega) = \psi(\omega)\tilde{y}(\omega)$ (see **SM VII**). For resonantly coupled oscillators, $\psi(\omega)$ is a complex function whose real and imaginary parts describe the expected phase relationships and transfer of energy between the oscillators (see **SM VII** and **FIGURE S6**). We determined the PerKy-38/p38 transfer function by taking >1,000 ratios between PerKy-38 and p38 Fourier spectra, $\psi(\omega) = \tilde{x}(\omega)/\tilde{y}(\omega)$. We find the PerKy-38/p38 transfer function is exactly predicted by describing the p38/PerKy-38 system as resonantly coupled oscillating biochemical reactions (**FIGURE 3A-C**; see **SM VII**, eq. S7.7). Fitting the transfer function extracts parameters of the resonant interaction, showing that damping of the system is weak [the total rate of spontaneous dephosphorylation, $\gamma = 0.00423 \pm 0.00009$ (SEM) hr^{-1}; see **SM V,** eq. S5.1 and **SM VI**, eq. S6.7.2] and that the Quality factor, Q, which measures the magnitude and specificity of amplification upon resonance, is high for such low frequency oscillations, $Q = 535 \pm 11$ (see **SM V**, eqs. S5.5, S5.6).

Activation of specific genetic responses through dynamic bioresonant stimulation

We hypothesized that the different frequencies present in p38 activation state oscillations resonate with other naturally occurring targets with corresponding natural frequencies to selectively drive specific responses to various stimuli. This immediately suggests that it should be possible to spoof the MAPK network to elicit specific genetic responses by periodically stimulating cells to force p38 activation state oscillations of a specific frequency. To test this hypothesis, we designed a pump system (**FIGURE S7**) to deliver sinusoidally varying concentrations of sorbitol to induce weak periodic osmotic shock with a predetermined frequency (see **FIGURES 1E,F**). Recall that in the case of hyperosmotic shock with sorbitol at constant concentration, where the p38 spectrum includes primarily $f_5 = 0.54$ hr^{-1}, we do not observe any PerKy-38 response. Conversely, we find when cells are stimulated by weakly oscillating hyperosmotic shock (sorbitol concentration between 0 – 40 mM) at PerKy-38's resonant frequency of $f = 0.36$ hr^{-1}, both the VPC and PerKy-38 activation state spectra include statistically significant peaks at that frequency (**FIGURE 3E**). Conversely, when VPC293 and PerKy293 cells are driven at off-resonant frequencies, we observe a signal at that frequency in VPC293 cells but no or very weak response in PerKy293 cells (**FIGURE 3D,F**), consistent with PerKy-38 activation due to bioresonance.

RNA sequencing demonstrates that cells driven by periodic osmotic shock exhibit radically altered gene expression profiles when driven at different frequencies compared to continuously osmotically shocked cells. We collected RNA from cells where for 48 hours the sorbitol concentration oscillated between 0 – 40 mM at a frequency of 0.36 hr^{-1} or 0.54 hr^{-1}, the two most statistically significant frequencies appearing in cells' Fourier spectra (**FIGURE 2K**). As controls, we also sequenced RNA from untreated negative controls, as well as samples treated with continuous exposure to sorbitol at 20 mM or 40 mM for 48 hours (the mean and maximum sorbitol

concentrations of the oscillations, respectively). Cluster analysis of genes we find to be differentially expressed relative to the negative control shows that the negative controls and the samples treated with continuous 20 mM and 40 mM sorbitol exhibit similar overall expression profiles (**FIGURE 4A**), indicating that the low sorbitol concentrations and mild osmotic shock imposed on the oscillatory samples are not, by themselves, sufficient to trigger a significantly altered gene regulatory response. Conversely, the expression profiles of cells driven by periodic stimulation differ dramatically from those treated with continuous stimulation, and from each other depending on the driving frequency (**FIGURES 4A-C**).

Enrichment analysis of genes uniquely differentially expressed when driven at different frequencies demonstrates that driving p38 oscillations at different frequencies activates different genetic programs, and, in particular, that driving p38 oscillations with only sugar at a frequency of 0.36 hr^{-1} induces an inflammation response typically associated with exposure to cytokines. We compared the lists of genes identified as differentially expressed when cells were driven at 0.54 hr^{-1} and 0.36 hr^{-1} to a list of differentially expressed genes identified from a group of samples obtained from cells driven at other frequencies from 0.09 hr^{-1} to 0.90 hr^{-1}, spaced at intervals of 0.09 hr^{-1} (**TABLE S1**). From this, we identified 195 genes that are uniquely differentially expressed when cells were driven at 0.36 hr^{-1} and 184 genes differentially expressed when cells were driven at 0.54 hr^{-1} (blue and red points in **Fig. 4B,C**, respectively**)**. Enrichment analysis of genes uniquely differentially expressed at 0.54 hr^{-1} (**TABLE S2**) generates only one statistically significant annotated pathway corresponding to Ras signaling (KEGG, $p_{adj} = 0.053$). Conversely, enrichment analysis of those genes uniquely differentially expressed in cells driven at 0.36 hr^{-1} (**TABLE S3**), a frequency which we found appears naturally in response to the cytokines IL-1β and TNF (**FIGURE 2K**), indicates that those genes are associated with MAPK responses to cytokines generally and interleukin and TNF signaling specifically, as well as inflammation, transcriptional regulation of cell death genes, and other processes known to be regulated by p38 (**FIGURE 4D** and **FIGURES S8-10**).

Intriguingly, we also find that genes differentially expressed when p38 oscillations are driven at a frequency of 0.36 hr^{-1} are associated with a variety of disease states with high significance, including cancer ($p_{adj} = 7.1 \times 10^{-5}$) and multiple neurodegenerative disorders including neuroinflammation, amyotrophic lateral sclerosis (ALS, $p_{adj} = 6.1 \times 10^{-3}$) and Alzheimer's disease ($p_{adj} = 5.1 \times 10^{-2}$), all of which have previously been associated with inappropriate p38 activity [**FIGURE 4E**, (*1, 4-11*)].

A theoretical framework describing bioresonance

To demonstrate the generality of bioresonance, we developed a mathematical framework to describe the effect of p38 oscillatory dynamics on downstream signaling pathways (see **SM V – SM IX**). A schematic is presented in **FIGURE 5**. We simulate p38 dynamics by extending a model describing p38 phosphorylation oscillations developed by Tomida *et al*. (*30*) to include interactions with upstream cascade components oscillating at different frequencies (*16, 22, 27*). This generates oscillations in p38 activation state whose spectrum is composed of stimulus-specific frequencies (orange lines in **FIGURE 5B-D)**. These p38 frequencies then resonantly drive oscillations in two downstream targets, each with a distinct natural frequency as a result of their individual interactions with other components. For each case, we use standard linear models of protein oscillations, *e.g.*, for p53 and Mdm2 [(*25*); see **SM VI**, **SM IX**]. Time traces of the resulting target oscillations (**FIGURE 5B-D**) show the bioresonance effect as amplification of selected

target oscillation amplitudes when the natural frequency of the selected target appears in the p38 spectrum. We further show that this specific target activation can be used to selectively control gene expression through standard models of transcriptional regulation by protein transcription factors (see **SM VIII**, **FIGURE S11**).

Discussion

Bioresonance provides a unique mechanism where, rather than requiring a bespoke enzyme of a particular conformation for every biochemical reaction, a single enzyme can be used to specifically control a broad range of targets without requiring alterations to its sequence or shape simply by altering the frequency with which its activation state oscillates. Upon activation, an enzyme that employs bioresonance can bind to and act upon all possible substrates, but only to a low level. However, each substrate can oscillate with a different natural frequency as a result of its other interactions in the cell, and only those substrates whose populations oscillate at the same frequency as the driving enzyme will be selectively amplified through bioresonance. As we show here, bioresonance is sufficient to provide selectivity between genetic responses, but this does not preclude additional allosteric or localization control mechanisms to enhance specificity.

Our theoretical description of bioresonance and the flow of a current of phosphates through the MAPK cascade (**FIGURE 5E**) matches that used to describe electronic alternating current (AC) circuits (**FIGURE 5F**), where resonance selectivity is frequently used as a control scheme. For example, in a radio receiver, a desired radio signal is selected from the multitude of transmitted signals by tuning the oscillatory frequency of an AC circuit within the receiver to be in resonance with the desired signal's electromagnetic wave oscillations. In the language of AC circuits, tuning the circuit to be in resonance with the radio wave minimizes the frequency-dependent impedance, $Z(\omega)$, given by the reciprocal of the transfer function of the circuit, $Z(\omega) \propto \psi^{-1}(\omega)$ (see **SM X**). This results in large amplitude current oscillations in the receiver that are decoded as audio information. The precision and degree with which the circuit can selectively amplify a given frequency signal is characterized by the Q factor, and the Q factor of the p38-PerKy-38 interaction, which operates at low milli- to microhertz frequencies, compares favorably to that of electronic components which typically operate at kilo- to megahertz frequencies.

Our results show that the p38 MAPK system, and potentially other oscillatory systems in the cell, function through a biochemical manifestation of the same resonance selectivity mechanism employed in AC circuits. As many MAPK cascade components have been observed to oscillate similarly to that described here for p38 and its substrates (*17-30*), the above arguments lead to the conclusion that the MAPK cascade functions as an oscillating current circuit, amplifying and distributing an electrical oscillating current of negatively charged phosphate residues to components at the end of the cascade responsible for directly controlling gene expression (see **SM X - IX** and **FIGURE 5G**). The magnitude of the phosphate current received by each terminal TF is determined by the product of the transfer functions, or the net impedance to the flow of phosphate current through each bioresonant element along the path (**FIGURE 5G;** see **SM XI**, eqs. S11.6 – S11.9). This, in turn, determines the degree to which genes regulated by those TFs are differentially expressed.

This correspondence with AC circuits suggests that other approaches used in AC electronic information encoding may also be employed by the cell. For example, heterodyning, where low-

frequency information is encoded in the beats of two combined high-frequency oscillators, could be used to frequency-shift oscillations from the short molecular time scales of chemical reactions to longer time scales relevant to cells or organisms.

Finally, we have demonstrated that this quantitative description and understanding of the bioresonant circuit properties of the MAPK cascade allows us to control the output of the cascade and resulting genetic responses using nothing more than sugar applied at different frequencies. We believe that this work unifies apparently disparate observations of oscillatory behavior of signaling components and altered gene expression (*17-30*) into a single coherent framework through which to understand, predict, and manipulate human gene expression. More work at the molecular level is needed to determine what mechanisms generate the stimulus-specific p38 frequencies and to determine what parameters, time delays, or other interactions set the frequencies with which p38 and its substrates oscillate (*39, 40*). We also note that our data (**FIGURE 4E**) suggest that many human diseases associated with p38 (*1, 7, 9-11, 41-52*) may result from inappropriate functioning of this bioresonance mechanism. As we demonstrate that it is possible to elicit different responses regardless of the precise chemical or physical nature of the stimulus, these findings may have implications for pharmaceutical development and strategies for modulating cell responses in a variety of diseases.

References and Notes

1. B. Canovas, A. R. Nebreda, Diversity and versatility of p38 kinase signalling in health and disease. *Nature Reviews Molecular Cell Biology* **22**, 346-366 (2021).
2. N. Trempolec, N. Dave-Coll, A. R. Nebreda, SnapShot: p38 MAPK substrates. *Cell* **152**, 924-924 e921 (2013).
3. J. Raingeaud *et al.*, Pro-inflammatory Cytokines and Environmental Stress Cause p38 Mitogen-activated Protein Kinase Activation by Dual Phosphorylation on Tyrosine and Threonine (∗). *Journal of Biological Chemistry* **270**, 7420-7426 (1995).
4. A. Lloret, T. Fuchsberger, E. Giraldo, J. Viña, Molecular mechanisms linking amyloid β toxicity and Tau hyperphosphorylation in Alzheimer′s disease. *Free Radic Biol Med* **83**, 186-191 (2015).
5. S. S. Holasek *et al.*, Activation of the stress-activated MAP kinase, p38, but not JNK in cortical motor neurons during early presymptomatic stages of amyotrophic lateral sclerosis in transgenic mice. *Brain Research* **1045**, 185-198 (2005).
6. M. Tortarolo *et al.*, Persistent activation of p38 mitogen-activated protein kinase in a mouse model of familial amyotrophic lateral sclerosis correlates with disease progression. *Mol Cell Neurosci* **23**, 180-192 (2003).
7. K. E. Medders, N. E. Sejbuk, R. Maung, M. K. Desai, M. Kaul, Activation of p38 MAPK is required in monocytic and neuronal cells for HIV glycoprotein 120-induced neurotoxicity. *J Immunol* **185**, 4883-4895 (2010).
8. K. E. Medders, M. Kaul, Mitogen-activated protein kinase p38 in HIV infection and associated brain injury. *J Neuroimmune Pharmacol* **6**, 202-215 (2011).
9. J. Gui *et al.*, Activation of p38α stress-activated protein kinase drives the formation of the pre-metastatic niche in the lungs. *Nat Cancer* **1**, 603-619 (2020).
10. L. García-Hernández *et al.*, The p38 MAPK Components and Modulators as Biomarkers and Molecular Targets in Cancer. *Int J Mol Sci* **23**, (2021).
11. J. C. Burton, W. Antoniades, J. Okalova, M. M. Roos, N. J. Grimsey, Atypical p38 Signaling, Activation, and Implications for Disease. *International Journal of Molecular Sciences* **22**, 4183 (2021).
12. S. Röhm *et al.*, Selective targeting of the αC and DFG-out pocket in p38 MAPK. *European Journal of Medicinal Chemistry* **208**, 112721 (2020).
13. M. T. Uhlik *et al.*, Rac-MEKK3-MKK3 scaffolding for p38 MAPK activation during hyperosmotic shock. *Nat Cell Biol* **5**, 1104-1110 (2003).
14. A. Plotnikov, E. Zehorai, S. Procaccia, R. Seger, The MAPK cascades: Signaling components, nuclear roles and mechanisms of nuclear translocation. *Biochimica et Biophysica Acta (BBA) - Molecular Cell Research* **1813**, 1619-1633 (2011).
15. Y. Ma, J. Nicolet, Specificity models in MAPK cascade signaling. *FEBS Open Bio* **13**, 1177-1192 (2023).
16. L. Sun, G. Yang, M. Zaidi, J. Iqbal, TNF-induced oscillations in combinatorial transcription factor binding. *Biochem Biophys Res Commun* **371**, 912-916 (2008).
17. H. Shankaran *et al.*, Rapid and sustained nuclear-cytoplasmic ERK oscillations induced by epidermal growth factor. *Mol Syst Biol* **5**, 332 (2009).
18. K. M. Waters, B. S. Cummings, H. Shankaran, N. E. Scholpa, T. J. Weber, ERK oscillation-dependent gene expression patterns and deregulation by stress response. *Chem Res Toxicol* **27**, 1496-1503 (2014).
19. B. Dérijard *et al.*, Independent human MAP-kinase signal transduction pathways defined by MEK and MKK isoforms. *Science* **267**, 682-685 (1995).

20. J. Raingeaud, A. J. Whitmarsh, T. Barrett, B. Dérijard, R. J. Davis, MKK3- and MKK6-regulated gene expression is mediated by the p38 mitogen-activated protein kinase signal transduction pathway. *Mol Cell Biol* **16**, 1247-1255 (1996).
21. J. Han *et al.*, Characterization of the structure and function of a novel MAP kinase kinase (MKK6). *J Biol Chem* **271**, 2886-2891 (1996).
22. L. S. Sorkin *et al.*, MKK3, an upstream activator of p38, contributes to formalin phase 2 and late allodynia in mice. *Neuroscience* **162**, 462-471 (2009).
23. A. Hoffmann, A. Levchenko, M. L. Scott, D. Baltimore, The IkappaB-NF-kappaB signaling module: temporal control and selective gene activation. *Science* **298**, 1241-1245 (2002).
24. M.-H. Sung *et al.*, Sustained Oscillations of NF-κB Produce Distinct Genome Scanning and Gene Expression Profiles. *PLOS ONE* **4**, e7163 (2009).
25. N. Geva-Zatorsky, E. Dekel, E. Batchelor, G. Lahav, U. Alon, Fourier analysis and systems identification of the p53 feedback loop. *Proceedings of the National Academy of Sciences* **107**, 13550-13555 (2010).
26. G. Lahav *et al.*, Dynamics of the p53-Mdm2 feedback loop in individual cells. *Nature Genetics* **36**, 147-150 (2004).
27. L. Sun, G. Yang, M. Zaidi, J. Iqbal, TNF-induced gene expression oscillates in time. *Biochem Biophys Res Commun* **371**, 900-905 (2008).
28. S. L. Werner, D. Barken, A. Hoffmann, Stimulus specificity of gene expression programs determined by temporal control of IKK activity. *Science* **309**, 1857-1861 (2005).
29. A. F. Peterson *et al.*, Systematic analysis of the MAPK signaling network reveals MAP3K-driven control of cell fate. *Cell Systems* **13**, 885-894.e884 (2022).
30. T. Tomida, M. Takekawa, H. Saito, Oscillation of p38 activity controls efficient pro-inflammatory gene expression. *Nature Communications* **6**, 8350 (2015).
31. H. Wu *et al.*, Activation of MEF2 by muscle activity is mediated through a calcineurin-dependent pathway. *Embo j* **20**, 6414-6423 (2001).
32. B. K. Chen *et al.*, PP2B-mediated dephosphorylation of c-Jun C terminus regulates phorbol ester-induced c-Jun/Sp1 interaction in A431 cells. *Mol Biol Cell* **18**, 1118-1127 (2007).
33. K. K. Hale, D. Trollinger, M. Rihanek, C. L. Manthey, Differential expression and activation of p38 mitogen-activated protein kinase alpha, beta, gamma, and delta in inflammatory cell lineages. *J Immunol* **162**, 4246-4252 (1999).
34. T. Nagai *et al.*, A variant of yellow fluorescent protein with fast and efficient maturation for cell-biological applications. *Nat Biotechnol* **20**, 87-90 (2002).
35. M. L. Markwardt *et al.*, An improved cerulean fluorescent protein with enhanced brightness and reduced reversible photoswitching. *PLoS One* **6**, e17896 (2011).
36. X. Gong, X. Ming, P. Deng, Y. Jiang, Mechanisms regulating the nuclear translocation of p38 MAP kinase. *Journal of Cellular Biochemistry* **110**, 1420-1429 (2010).
37. P. R. Young *et al.*, Pyridinyl imidazole inhibitors of p38 mitogen-activated protein kinase bind in the ATP site. *J Biol Chem* **272**, 12116-12121 (1997).
38. H. S. Lawson, G. Holló, R. Horvath, H. Kitahata, I. Lagzi, Chemical Resonance, Beats, and Frequency Locking in Forced Chemical Oscillatory Systems. *The Journal of Physical Chemistry Letters* **11**, 3014-3019 (2020).
39. Y. Zhang, H. Liu, F. Yan, J. Zhou, Oscillatory dynamics of p38 activity with transcriptional and translational time delays. *Scientific Reports* **7**, 11495 (2017).
40. D. Bratsun, D. Volfson, L. S. Tsimring, J. Hasty, Delay-induced stochastic oscillations in gene regulation. *Proceedings of the National Academy of Sciences* **102**, 14593-14598 (2005).

41. C. Atzori *et al.*, Activation of the JNK/p38 pathway occurs in diseases characterized by tau protein pathology and is related to tau phosphorylation but not to apoptosis. *Journal of Neuropathology & Experimental Neurology* **60**, 1190-1197 (2001).
42. S. Colié *et al.*, Neuronal p38α mediates synaptic and cognitive dysfunction in an Alzheimer's mouse model by controlling β-amyloid production. *Sci Rep* **7**, 45306 (2017).
43. I. Darlyuk-Saadon *et al.*, Expression of a constitutively active p38α mutant in mice causes early death, anemia, and accumulation of immunosuppressive cells. *The FEBS Journal* **288**, 3978-3999 (2021).
44. M. S. Gee *et al.*, A selective p38α/β MAPK inhibitor alleviates neuropathology and cognitive impairment, and modulates microglia function in 5XFAD mouse. *Alzheimers Res Ther* **12**, 45 (2020).
45. K. Hensley *et al.*, p38 Kinase Is Activated in the Alzheimer's Disease Brain. *Journal of Neurochemistry* **72**, 2053-2058 (1999).
46. G. Kheiri, M. Dolatshahi, F. Rahmani, N. Rezaei, Role of p38/MAPKs in Alzheimer's disease: implications for amyloid beta toxicity targeted therapy. *Reviews in the Neurosciences* **30**, 9-30 (2019).
47. J. K. Lee, N. J. Kim, Recent Advances in the Inhibition of p38 MAPK as a Potential Strategy for the Treatment of Alzheimer's Disease. *Molecules* **22**, (2017).
48. L. Munoz, A. J. Ammit, Targeting p38 MAPK pathway for the treatment of Alzheimer's disease. *Neuropharmacology* **58**, 561-568 (2010).
49. J. G. Sheng *et al.*, Interleukin-1 promotion of MAPK-p38 overexpression in experimental animals and in Alzheimer's disease: potential significance for tau protein phosphorylation. *Neurochemistry international* **39**, 341-348 (2001).
50. A. Sun, M. Liu, X. V. Nguyen, G. Bing, P38 MAP kinase is activated at early stages in Alzheimer's disease brain. *Experimental Neurology* **183**, 394-405 (2003).
51. V. I. Viorel, Y. Pastorello, N. Bajwa, M. Slevin, p38-MAPK and CDK5, signaling pathways in neuroinflammation: a potential therapeutic intervention in Alzheimer's disease? *Neural Regeneration Research* **19**, 1649-1650 (2024).
52. X. Zhu *et al.*, Activation of p38 Kinase Links Tau Phosphorylation, Oxidative Stress, and Cell Cycle-Related Events in Alzheimer Disease. *Journal of Neuropathology & Experimental Neurology* **59**, 880-888 (2000).
53. J. Han, J. Wu, J. Silke, An overview of mammalian p38 mitogen-activated protein kinases, central regulators of cell stress and receptor signaling. *F1000Res* **9**, (2020).
54. C. A. Schneider, W. S. Rasband, K. W. Eliceiri, NIH Image to ImageJ: 25 years of image analysis. *Nature Methods* **9**, 671-675 (2012).
55. D. R. Stirling *et al.*, CellProfiler 4: improvements in speed, utility and usability. *BMC Bioinformatics* **22**, 433 (2021).
56. M. I. Love, W. Huber, S. Anders, Moderated estimation of fold change and dispersion for RNA-seq data with DESeq2. *Genome Biology* **15**, 550 (2014).
57. L. Kolberg *et al.*, g:Profiler—interoperable web service for functional enrichment analysis and gene identifier mapping (2023 update). *Nucleic Acids Research* **51**, W207-W212 (2023).
58. L. Bintu *et al.*, Transcriptional regulation by the numbers: applications. *Curr Opin Genet Dev* **15**, 125-135 (2005).
59. L. Bintu *et al.*, Transcriptional regulation by the numbers: models. *Curr Opin Genet Dev* **15**, 116-124 (2005).
60. V. Martin, F. Zhuang, Y. Zhang, K. Pinheiro, R. Gordân, High-throughput data and modeling reveal insights into the mechanisms of cooperative DNA-binding by transcription factor proteins. *Nucleic Acids Research* **51**, 11600-11612 (2023).

Acknowledgments: We thank Nigel Goldenfeld, Edward C. Cox, Hernan Garcia, Joseph Rudnick, Matthew Scott, Zhenyu Jia, and Nathan Gabor for useful discussions.

Funding:

Startup funds provided by University of California, Riverside (TEK)
UCR School of Medicine, Dean's Collaborative Seed Grant (TEK, MK, RZ)
University of California Office of the President UC Multicampus Research Programs and Initiatives grant M21PR3267 (TEK, MK, RZ)
National Science Foundation, NSF DMR-2131963 (RZ)
National Institute of Health NIH, R01 DA052209 (MK)

Author contributions:

Conceptualization: MK, RZ, TEK
Methodology: MW, SN, DO, SA, PM, AN, SL, MG, SO, MK, RZ, TEK
Investigation: MW, SN, DO, SA, PM, AN, SL, AA, KY, MG, NY, SO, MK, RZ, TEK
Visualization: MW, SN, DO, PM, SL, AA, KY, NY, AEN, TEK
Funding acquisition: MK, RZ, TEK
Project administration: MK, RZ, TEK
Supervision: MK, RZ, TEK
Writing – original draft: MW, TEK
Writing – review & editing: MW, SN, SL, KY, SO, MK, RZ, TEK

Competing interests: Authors declare that they have no competing interests.

Data and materials availability: RNAseq data are available from the Sequence Read Archive (SRA, BioProject PRJNA1225323) and Gene Expression Omnibus (GEO, GSE289999). Code used for analysis and simulation is available at https://github.com/kuhlman-lab-ucr/p38. PerKy-38 was provided under Material Transfer Agreement (MTA) with Dr. Taichiro Tomida and Dr. Atsushi Miyawaki. Plasmids pB510B-1 and pB210PA-1 for piggybac-mediated stable transfection are restricted from distribution under purchase agreement with Systems Biosciences. The plasmid pUC57-kan-VPC is available upon request to thomas.kuhlman@ucr.edu and can be transferred under MTA with UC Riverside.

FIGURES

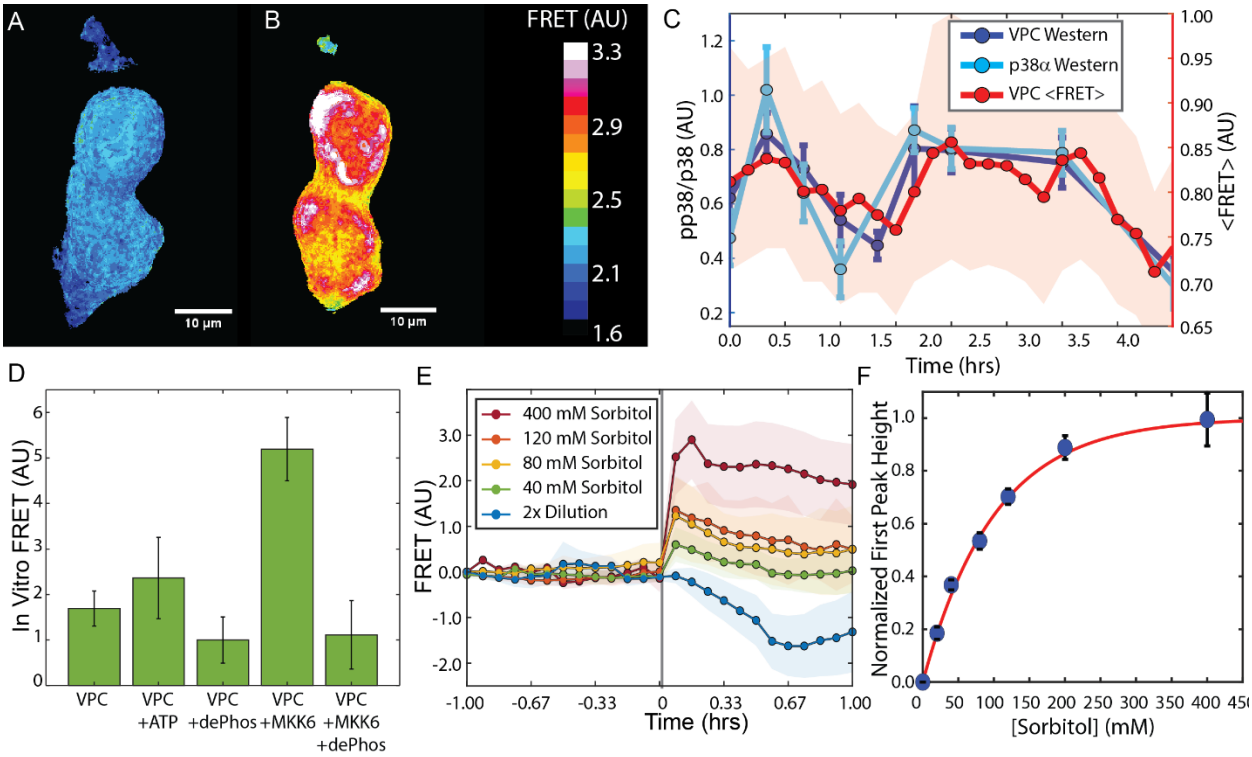

Fig. 1. VPC, a direct FRET-based reporter of p38 activation state. (**A**) FRET state of two resting HEK-293T cells expressing VPC (VPC293). (**B**) The same two cells, immediately after hyperosmotic shock induced by the addition of 120 mM sorbitol. (**C**) VPC (dark blue, from VPC293 cells) and p38α (light blue, from untransfected HEK-293T cells) phosphorylation dynamics measured using Western blot and ensemble-averaged FRET (red, $N \approx 1{,}500$ cells). Shaded region is the 95% confidence bound for FRET data, while error bars are standard deviation of three biological western blot replicates. See **Fig. S1** for example western blots. (**D**) In vitro FRET of purified VPC protein; as purified (VPC), + 0.25 mM ATP-Mg (VPC +ATP), VPC + 0.25 mM ATP-Mg + 100 U/ml Antarctic Phosphatase (VPC +dePhos), VPC + 0.25 mM ATP-Mg + 200 nM MKK6 kinase (VPC +MKK6), and VPC + 0.25 mM ATP-Mg + 200 nM MKK6 kinase + 100 U/ml Antarctic Phosphatase. Values are means of 15 measurements, error bars are SEM. (**E**) Dynamic ensemble averaged FRET response of VPC293 cells upon hyperosmotic (Green: 40 mM, Orange: 80 mM, Blue: 120 mM sorbitol) or hypoosmotic (Red: 2x dilution with ultrapure H_2O) shock. Shock was induced at $t = 0$, indicated by the vertical gray line. Points: average of three biological replicates, shaded region indicates 95% confidence bounds. (**F**) Normalized height of the first peak in the VPC FRET signal upon induction of hyperosmotic shock via the addition of sorbitol, as in (E). Blue points: mean of three biological replicates, error bars: standard deviation. Red line is best fit to the function $1 - e^{-b*[\text{Sorbitol}]}$, with the best fit value of $b = 0.01 \pm 0.002$ mM^{-1}. Hyperosmotic shock with 400 mM sorbitol results in cell death.

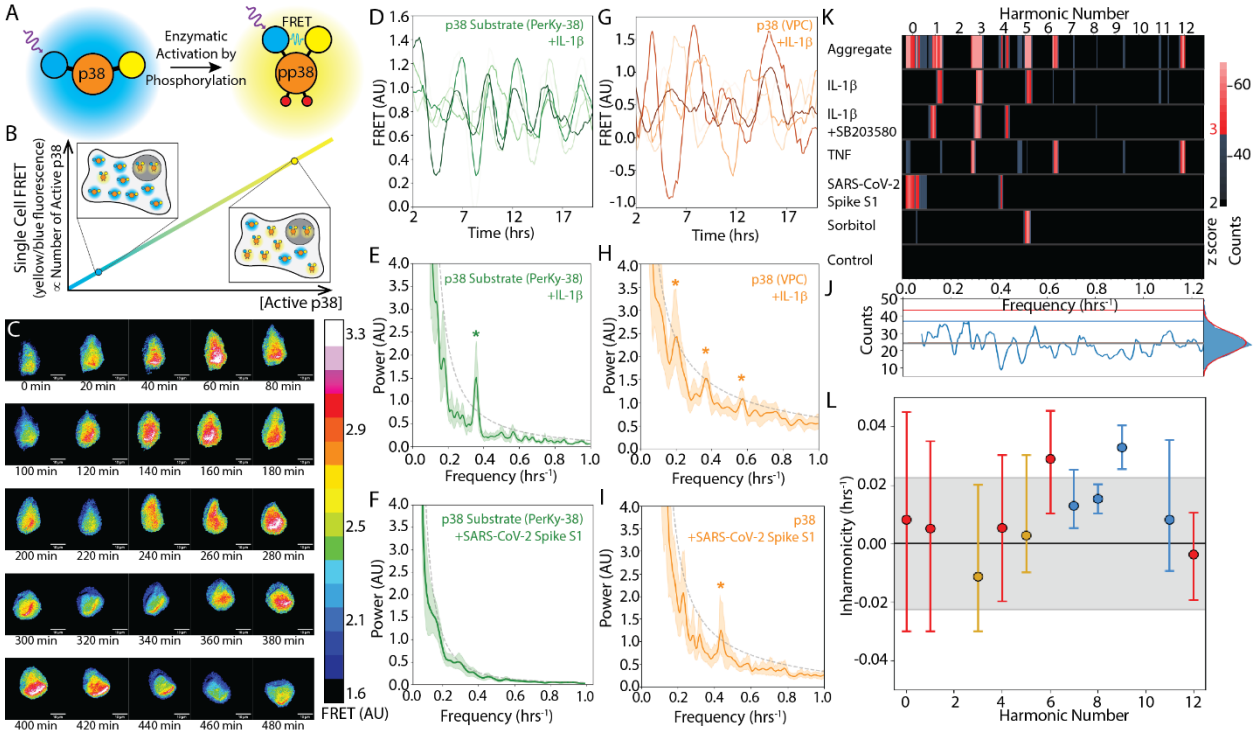

Fig. 2. PerKy-38 and p38 exhibit phosphorylation state oscillations with stimulus-specific frequencies. (**A-B**) Interpretation of single cell FRET signals. (**A**) Activation of a p38 protein by phosphorylation discretely increases the FRET signal from that molecule. (**B**) Individual cells contain many p38 molecules, hence the single cell FRET signal is proportional to the number of active p38 molecules. (**C**) Oscillating p38 activation state shown for a single VPC293 cell stimulated by hyperosmotic shock with sorbitol. The first image (t = 0) is 35 hours after addition of 120 mM sorbitol. (**D**) FRET time traces of five fields of view (FOVs) of PerKy293 cells + 300 ng/mL IL-1β. (**E**) Ensemble averaged Fourier spectrum of 70 FOVs of PerKy293 [as in (D)]. Shaded region: 95% confidence bounds; dashed gray line: 99% confidence interval for peak magnitudes. Asterisks: statistically significant peaks. (**F**) Ensemble averaged Fourier power spectrum of 100 FOVs of PerKy293 cells exposed to 2 nM SARS-CoV-2 Spike S1. Note the absence of statistically significant peaks. (**G**) FRET time traces of five FOVs of VPC293 cells + 300 ng/mL IL-1β. (**H**) Ensemble averaged Fourier spectrum of 66 FOVs of VPC293 cell line [as in (G)]. Asterisks: statistically significant peaks. Gray dashed line: 99% confidence level. (**I**) Ensemble averaged Fourier power spectrum of 70 FOVs of VPC293 cells exposed to 2 nM SARS-CoV-2 Spike S1 protein. Note statistically significant peak at $f = 0.45 \pm 0.01$ hr^{-1} ($p = 2.3 \times 10^{-4}$, marked with asterisk), with no significant peak at $f = 0.36$ hr^{-1}. (**J**) Statistics of local maxima in Fourier spectra of unstimulated VPC293 cells (see **SM II**). Integration over frequency yields a normal distribution (right) used to quantify z score; z = number of standard deviations from mean. Gray: mean; blue: $z = 2$; red: $z = 3$. (**K**) Oscillatory frequencies in individual cells for different stimuli. Top: aggregated spectrum. Expected frequencies of the nth harmonic [$f_n = (n + 1)f_0$, $n = 0, 1, 2, \ldots$, and $f_0 = 0.09$ hr^{-1}] indicated. Blue: $2 \leq z < 3$ and red: $z \geq 3$. (**L**) Inharmonicity of identified frequencies. Points: band center of mass, error bars: band width at z score boundary. Blue: $2 \leq z < 3$; red: $z \geq 3$; yellow: $z > 10$. Gray shaded region: interval of $\pm f_0/4$ (see **SM III**).

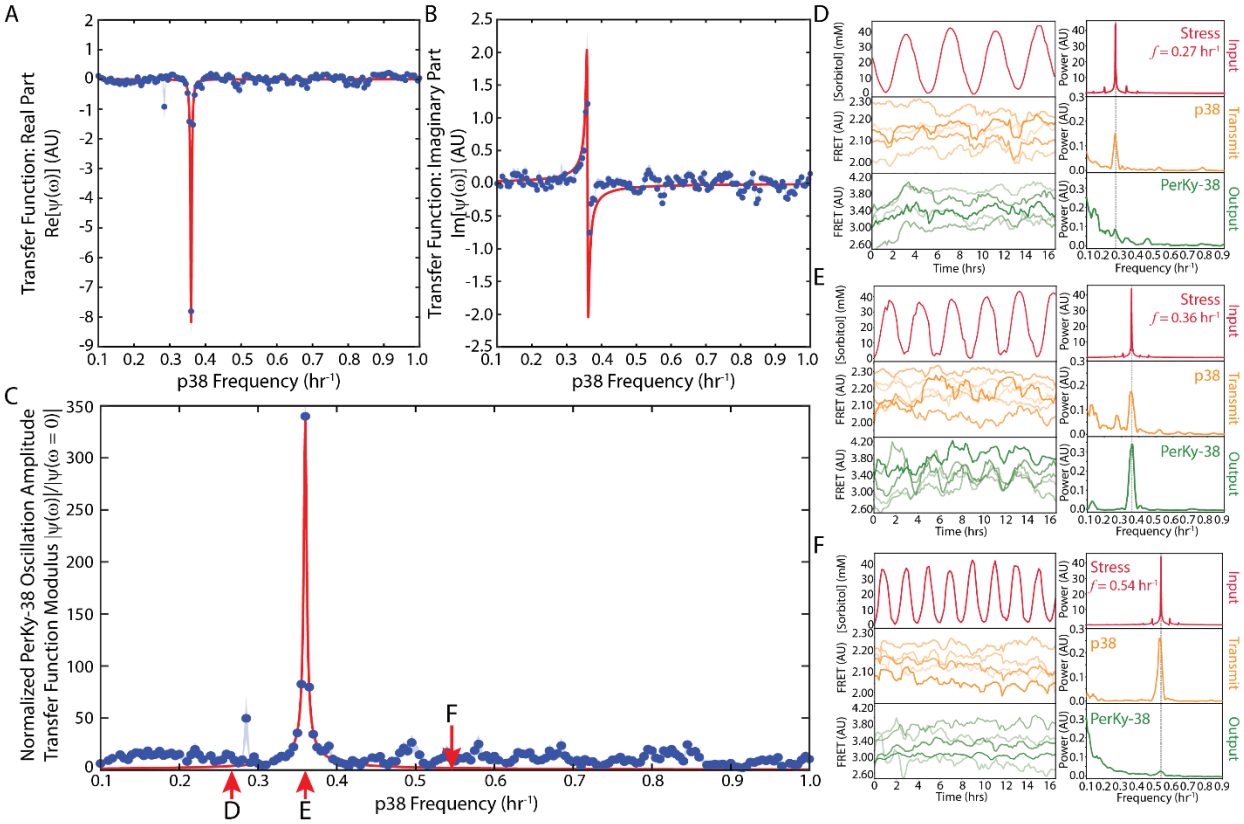

Fig. 3. p38 drives target activation through forced resonant oscillations. Real (**A**) and Imaginary (**B**) parts of the transfer function, $\psi(\omega)$, between p38 [$\tilde{y}(\omega)$] and PerKy-38 [$\tilde{x}(\omega)$], $\psi(\omega) = \tilde{x}(\omega)/\tilde{y}(\omega)$, see **SM VII**, and **Fig. S6**. Blue points: data, $N = 1{,}092$ ratios of Fourier spectra from VPC293 and PerKy293 cells; blue shaded region: 95% confidence region; red lines: fits to expected form of the transfer function of a driven simple harmonic oscillator; see **SM VII**, eqs. S7.3, S7.7; *cf.* **Fig. S6A,B**. (**C**) Normalized modulus of the transfer function between p38 and PerKy-38, showing PerKy-38 amplitude response as a function of p38 driving frequency, see **SM V**, eq. S5.3, and **SM VII**, eq. S7.8; *cf.* **Fig. S6C**. Fits yield damping parameter $\gamma = 0.00423 \pm 0.00009$ (SEM) hr^{-1}, quality factor, $Q \equiv \omega_0/\gamma = 535 \pm 11$. (**D-F**) Driving the p38 MAPK system with periodic hyperosmotic shock. Time series (left) and Fourier spectra (right) of the input sorbitol flow (red, top, measured by rhodamine B fluorescence), p38 response (orange, middle, VPC FRET), and PerKy-38 output (green, bottom, PerKy-38 FRET) when cells are subjected to periodic hyperosmotic stress by oscillatory flow of sorbitol between 0 mM and 40 mM at a frequency of (**D**) 0.27 hr^{-1}, (**E**) 0.36 hr^{-1}, and (**F**) 0.54 hr^{-1}. The corresponding driving frequencies relative to the modulus of the transfer function are indicated by red arrows in (C).

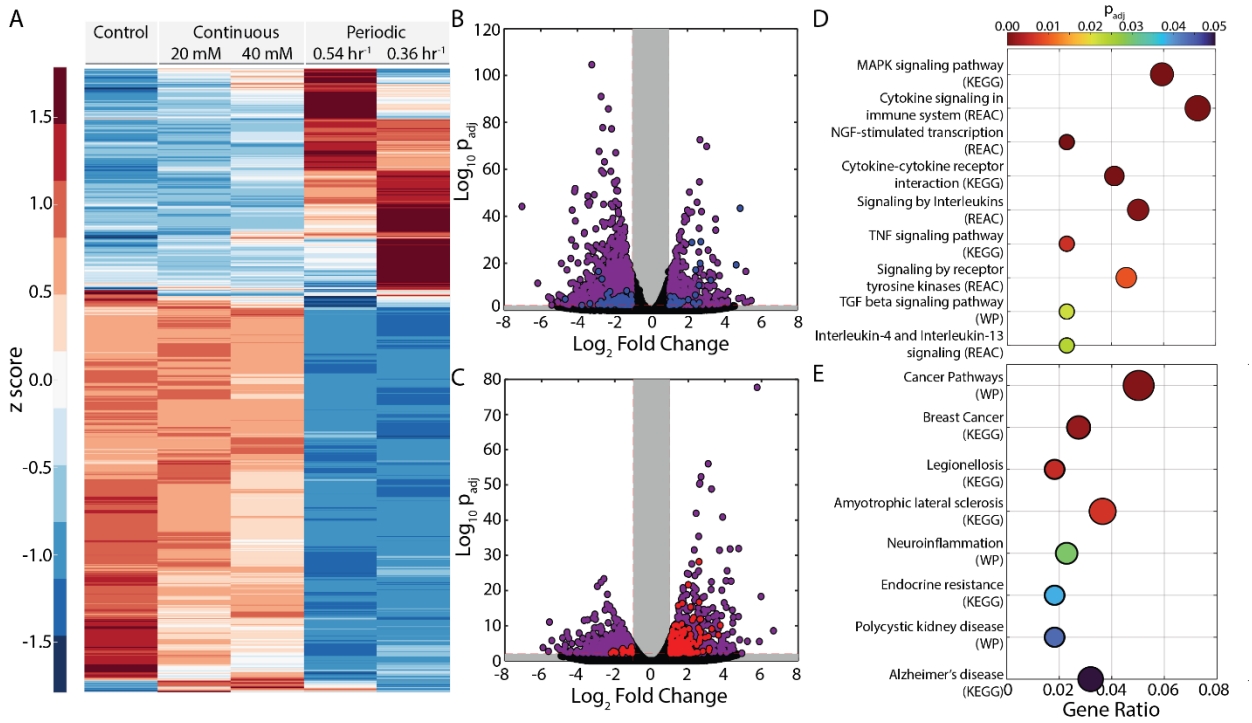

Fig. 4. Activation of specific genetic responses through dynamic bioresonant stimulation. (**A**) Clustergram of expression levels of 3,336 identified statistically significantly ($p_{adj} < 0.01$) differentially expressed [$|\log_2(\text{fold change})| > 1$] genes as determined by RNA sequencing of untreated negative control samples (Control), samples osmotically stressed with continuously applied sorbitol [20 mM or 40 mM], and samples driven with sorbitol oscillating between 0 – 40 mM at a frequency of either 0.54 hr^{-1} or 0.36 hr^{-1}, as in **Fig. 3D-F**. All RNAseq was performed with two biological replicates of each sample. (**B** – **C**) Volcano plots of RNAseq results from samples periodically driven at a frequency of 0.54 hr^{-1} (**B**) and 0.36 hr^{-1} (**C**). Purple points: genes differentially expressed regardless of driving frequency (N = 1,144); blue points: genes differentially expressed only at driving frequency of 0.54 hr^{-1} (N = 184); red points: genes differentially expressed only at driving frequency of 0.36 hr^{-1} (N = 195). (**D** – **E**) Terms resulting from enrichment analysis of genes uniquely expressed at a driving frequency of 0.36 hr^{-1} [red points in (C)] for (**D**) regulatory pathways and (**E**) disease-related pathways. Data sources include KEGG, Reactome (REAC) and WikiPathways (WP). Point size linearly increases with the number of genes, from 5 - 20, intersecting with the term. Terms displayed here are filtered for brevity and relevance; complete lists of enriched terms are given in **Figs. S8-S10**.

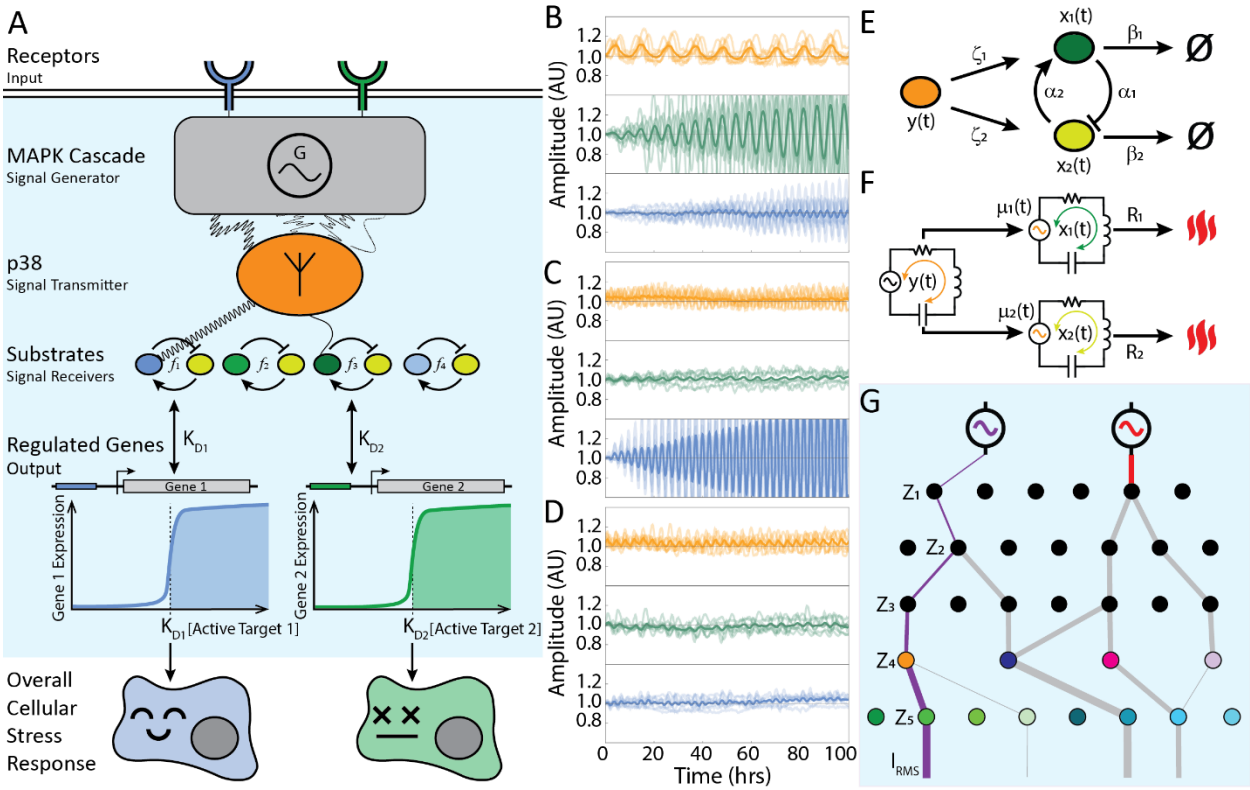

Fig. 5. An Integrated Conceptual Framework Describing MAPK Bioresonance and Output. (**A**) When stimuli are received by the cell, receptors activate the MAPK cascade, which we treat as a "black box" signal generator (generator symbol) that sinusoidally drives p38 oscillations (orange oval) at different frequencies. p38 functions as a transmitter (antenna symbol) whose oscillatory frequencies resonantly drive oscillations of downstream targets (green, blue, and yellow ovals), which we model as two-component biological oscillators with some natural frequencies f_i. Resonantly activated substrates then activate or repress genes regulated by those substrates. The combined changes in gene expression lead to the overall correct (blue) or incorrect (green) cellular stress response. (**B - D**) Simulated time traces of p38 (orange) resonantly interacting with two downstream targets, Substrate A and Substrate B, with natural frequencies $f_A = 0.18$ hr^{-1} (green) and $f_B = 0.36$ hr^{-1} (blue). Shown are examples with: (**B**) p38 driven at $f = 0.09$ hr^{-1}, which generates harmonics on-resonance with Substrate A; (**C**): p38 driven at $f = 0.36$ hr^{-1}, on-resonance with Substrate B; (**D**) p38 driven at $f = 0.27$ hr^{-1}, off-resonance with both substrates. Transparent lines: individual simulations; solid lines: mean of 7 simulations simulating one FOV. Fourier spectra are averages of 14 simulated FOVs; see **SM IX**. (**E**) A quantitative model of p38 [$y(t)$ orange] driving oscillations in two interacting TFs [$x_i(t)$, green and yellow]. TFs are phosphorylated with rates ζ_i; TFs react with each other with rates α_i; TFs spontaneous dephosphorylate (null symbol) with rates β_i. See **SM VI**. (**F**) Equivalent representation of (E) in terms of AC circuit elements, oscillating phosphate current in p38 (orange) inducing chemical potentials, $\mu_i(t)$, in downstream TFs, with spontaneous dephosphorylation analogous to resistive heat losses. See **SM VI** and **SM X – XI**. (**G**) Representation of the MAPK cascade as a phosphate current amplifier and distribution network. Phosphate currents (I_{RMS}, lines) are amplified or suppressed along paths through the cascade based upon the net frequency-dependent impedance, Z, of each MAPK element (circles) along each path.